Received: 13 June 2024 | Revised: 19 September 2024 | Accepted: 19 October 2024

IET Generation, Transmission & Distribution

DOI: 10.1049/gtd2.13313

The Institution of Engineering and Technology WILEY

ORIGINAL RESEARCH

Resilience assessment of power transmission system during wildfire disasters considering spread process

Shengwen Shu[1] | **Nan Xiao**[1] | **Shiyun Cao**[1] | **Jun Xu**[2] | **Caoying Fang**[2] | **Wenbing Xie**[2]

[1]College of Electrical Engineering and Automation, Fuzhou University, Fuzhou, People's Republic of China

[2]Electric Power Research Institute, State Grid Fujian Electric Power Co., Ltd, Fuzhou, People's Republic of China

Correspondence
Shengwen Shu, College of Electrical Engineering and Automation, Fuzhou University, Fuzhou, People's Republic of China.
Email: shushengwen@fzu.edu.cn

Funding information
National Natural Science Foundation of China, Grant/Award Number: 52207150

Abstract

Large-scale wildfires can significantly reduce the air gap insulation resistance of high-voltage transmission lines and cause chain tripping incidents. To assess the resilience of the power transmission system during wildfire, this paper proposes a resilience assessment framework for transmission system that considers the entire process of wildfire disaster. Firstly, a wildfire spread model, considering multiple influencing factors, is developed based on the cellular automaton. Based on the air gap breakdown mechanism during wildfires, the trip-out probability of transmission lines is calculated, and various failure scenarios are obtained by using the Monte Carlo sampling. Secondly, considering the geographical location of failures, maintenance personnel schedules and restoration time, a power transmission system restoration model is established. Thus, a resilience assessment method for power transmission system during wildfire disasters is proposed. Finally, IEEE RTS-79 transmission system is taken as an example to demonstrate the effectiveness of the proposed resilience assessment method. The results show that the proposed method can effectively calculate the wildfire spread tendency and transmission line's trip-out probability. Furthermore, three typical resilience improvement measures are quantitatively analysed, which provides a quantifiable reference for the power sector to formulate prevention and recovery strategies for extreme wildfire disasters.

1 | INTRODUCTION

Long-distance transmission of electric energy is inevitable due to the rapid development of economy and society. Worldwide, there is an increasing number of transmission line tripping and outage incidents brought on by wildfires [1, 2]. Wildfires have become a big threat to the safety and stability of transmission lines [3, 4]. The notion of resilience was developed to measure the ability of power transmission system to withstand and recover from extreme disasters such as wildfires [5–7]. It has become a top priority to study the power transmission system's resilience assessment tools and formulate the resilience improvement strategy for the system to cope with the increasingly frequent wildfire disasters.

Many studies conducted recently have focused on evaluating and enhancing the resilience of power transmission, distribution and substation systems during extreme weather conditions such as typhoons [8], ices [9], wildfires [10], floods [11], windstorms [12], hurricanes [13], and earthquakes [14]. Although wildfire is a frequently occurring natural catastrophic event and seriously threatening the normal operation of power transmission and distribution systems, limited investigations have focused on the resiliency assessment and its improvement measures. Aiming at enhancing the resilience of power distribution networks, methods to optimize the operating modes such as network reconfiguration [15], microgrids, demand response (DR), distributed energy resources (DERs) [16, 17], and optimal load shedding [18] are most investigated. In [15], resilience of a distribution network is evaluated considering the effect of urban wildfires, and network is reconfigured by finding the optimal switching sequence that enhances the resilience of the distribution network. In [16–18], the resilience of the power distribution

network is assessed during a progressing wildfire and shown to be enhanced through optimal energy dispatch, and microgrids, DR and DERs concepts. A microgrid-based strategy for managing wildfire risks and preventing blackouts has been proposed in [18]. A study on the effects of power line height and wildfire distance from power lines, along with a fire growth model, have been conducted in [19] to examine the resilience of power transmission systems caused by wildfires.

Since the spread characteristics of wildfires and probability of transmission line failures are key to assess the resilience of power transmission systems, some wildfires spread models and failure probability calculation models have been proposed by considering topography, weather elements, fuel loads, vegetational heights, and structural and electrical variables of transmission lines. At present, the most commonly used empirical and semi-empirical models for wildfires spread include the American Rothermel model based on energy conservation [20], the Canadian national forest fire spread model [21], the Australian McArthur model [22], and the Chinese Wang Zhengfei model [23]. To accurately calculate the failure probability of transmission lines caused by wildfires, experiments have been carried out to determine the breakdown voltage of air in the presence of a typical vegetation flame [24–26]. In [27, 28], the probability of wildfire ignition caused by the heating and cooling processes of electrical power conductors has been studied. Additionally, the breakdown probability of air as a function of transmission line height and wildfire distance from transmission lines has been investigated [29].

There have been some studies on the resilience assessment and improvement measures of power transmission system under extreme weather conditions. However, quantitative assessment of power transmission system's resilience during wildfire disasters considering the entire spread process and the impact of zone structure of flame on the trip-out probability of transmission lines are inadequate. The following are some research gaps that need further investigation:

1. The existing wildfire spread models only consider the impact of environmental factors such as temperature and humidity, wind speed and direction, and slope and combustible type on the spread of wildfires. However, few important factors such as combustible humidity and vegetation height are ignored.
2. The existing probability models of transmission line trip-out caused by wildfires are oversimplified, and did not considered the effects of flame zone on both phase-to-ground and phase-to-phase faults.
3. Also, the existing resilience assessment models have simplified system recovery model, which did not consider the spatial relationships between repair resources, power system components and maintenance departments.

To fill the aforementioned gaps, this paper proposes a quantitative resilience assessment model for power transmission system during wildfire disasters considering the entire spread process. The major contributions of this paper are as follows:

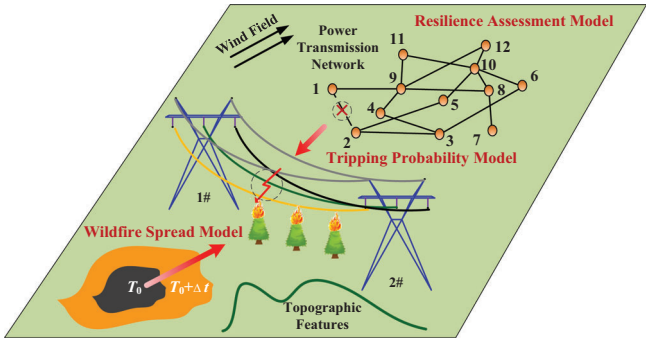

FIGURE 1 Resilience assessment framework for transmission system during wildfire disasters.

1. Through the incorporation of combustible humidity and vegetation height into the Wang Zhengfei model, a cellular automaton-based improved wildfire spread model is established. The initial spread speed of wildfires is corrected in the model by introducing combustible humidity. The wildfire spread processes under different influencing factors are compared based on the improved model. Further, a practical example is provided to demonstrate the wildfire spread model.
2. By dividing the air gap between the transmission line and vegetation under wildfire into flame region, smoke region and ion region, a refined probability model for transmission line trip-out caused by wildfires synthesizing phase-to-ground and phase-to-phase faults is established. The change in trip-out probability of transmission lines caused by phase-to-ground and phase-to-phase faults with different vegetation types and heights is calculated.
3. A transmission system resilience assessment framework that considers the entire wildfire spread process is proposed by establishing a refined post disaster recovery model. The resilience of power transmission system during wildfire disasters considering different rated voltages, vegetation heights and pre-disaster load transfer strategies is quantified. Specifically, three resilience improvement measures are analysed for power transmission system during wildfire disasters.

The rest of this paper is organized as follows. Section 2 describes the mathematical model of wildfire spread, transmission lines' trip-out probability during the wildfire disasters and the resilience assessment model. Results of wildfire spread, transmission lines' trip-out probability and resilience assessment model for transmission system are presented in Section 3. Finally, Section 4 concludes the paper.

2 | ASSESSMENT MODEL AND FORMULATIONS

2.1 | Assessment framework

The overall framework of resilience assessment for power transmission system during wildfire disasters is illustrated in Figure 1.

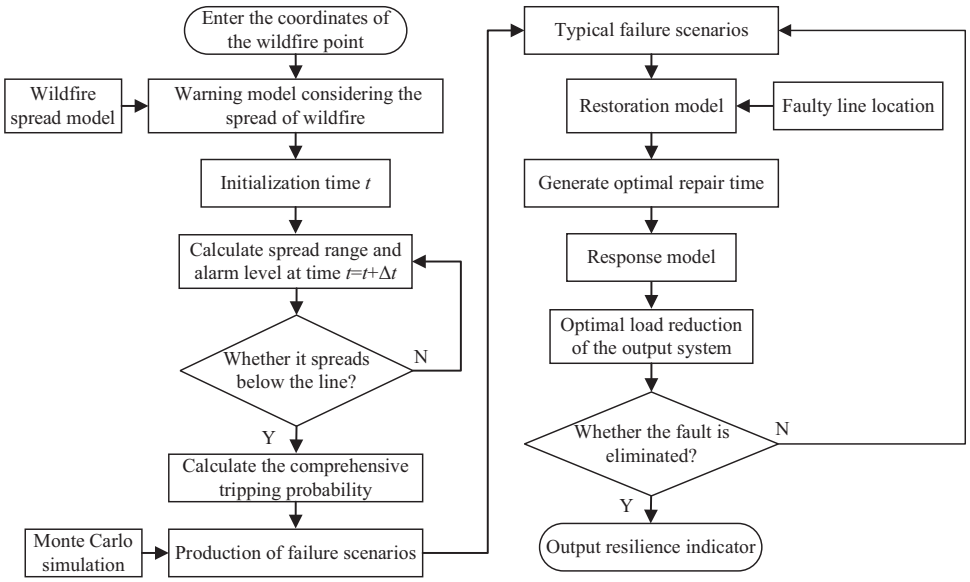

FIGURE 2 Resilience assessment process for transmission system during wildfire disasters.

The framework consists of wildfire spread model, tripping probability model of transmission line and resilience assessment model of transmission system. Resilience assessment process for transmission system during wildfire disasters is depicted in Figure 2.

2.2 | Wildfire spread model

2.2.1 | Initial spread speed

The initial spread speed of a wildfire, R_0 is defined on a levelled and windless surface. According to Wang Zhengfei's model, the initial spread speed depends on the environmental conditions such as temperature and humidity as,

$$R_0 = 0.03q + 0.01h - 0.3 \tag{1}$$

where q represents the temperature, °C; h represents the minimum relative humidity, %.

The initial spread speed also depends on the humidity of the fuel, which determines the difficulty of its combustion. The Wang Zhengfei's model only considers the environmental factors including temperature and humidity, which causes a big discrepancy between the estimated results and the actual scenarios. Therefore, the factor of combustible humidity is introduced in this paper to establish a relationship between the initial spread speed and the combustible humidity, temperature and humidity as [30],

$$R_0 = -1.629 + 0.133q - 0.022h + 0.087m \tag{2}$$

where m is the humidity of combustible material, %.

In general, extracting the humidity of combustible materials is difficult. Considering that the humidity of combustible materials largely depends on the environmental factors, the humidity can be calculated using an empirical formula as [31],

$$m = 57.06 + 0.987h - 41.02 \lg q \tag{3}$$

TABLE 1 Combustible coefficient for different vegetation types.

Vegetation types	Grass	Cedar	Straw	Grassland	Pine needle
K_s	0.9	0.8	0.6	0.5	0.4

2.2.2 | Wind speed and direction coefficient

The wind speed and direction influence the spread speed of wildfires, while the wind speed and direction coefficient is defined as [32],

$$K_w = 0.1783 v_w \cos\gamma \tag{4}$$

where v_w is wind speed, m/s; γ is the angle between wind direction and spread direction.

2.2.3 | Combustible coefficient

Vegetation can be divided into combustible and non-combustible types. The combustible coefficient in Table 1 illustrates how different vegetation types have varying effects on the spread of wildfires.

2.2.4 | Vegetation height coefficient

When the effective fuel load of a forest doubles, the fire spread speed will double while the fire intensity will increase by four

times. Assuming that the normal combustion is maintained because of fuel density fuel load and fire spread speed will increase as the vegetation height increases. Assuming the vegetation height is D_z, based on the fitting results of the spread speed for different vegetation heights, it can be inferred that the height coefficient of grassland shrubs is [33],

$$K_z = 1.26922 D_z^{0.10773} \tag{5}$$

The height coefficient of trees is,

$$K_z = 0.7036 + 0.82\left(1 - e^{-\frac{D_z}{4.46}}\right) \tag{6}$$

2.2.5 | Slope coefficient

The spread speed of wildfires is influenced by the uphill and downhill slopes, as well as the steepness of the slope. The pace at which wildfires spread rises when travelling uphill ($G = 0$); conversely, the speed at which they spread slows down when travelling downhill ($G = 1$). Assuming the slope is φ, the slope coefficient is defined as,

$$K_\varphi = e^{3.533(-1)^G |\tan\varphi|^{1.2}} \tag{7}$$

Combining the initial spread speed and four adjustment coefficients, the spread speed of wildfires can be calculated as,

$$R = R_0 K_w K_s K_z K_\varphi \tag{8}$$

2.2.6 | Cellular automata model

Selecting a cellular automaton model to simulate the spread of wildfires, the state change of each tree is solely dependent on its current state and the state of the tree (N) in the Moore neighbourhood. Among them, the conversion rule $S^{t+\Delta t} = f(S^t, N)$ is the core that drives the entire system's operation, and $N = 8$ is the Moore domain. Each grid with corresponding row and column numbers is a cell. Each cell has its own state at any moment. Cell states can be transformed based on transformation rules, which use the current state of the cell as well as the states of its neighbouring cells to determine the dynamic function of the cell state at the next moment. During the simulation process, the neighbourhood changes are calculated dynamically and iteratively based on the transformation rules [34].

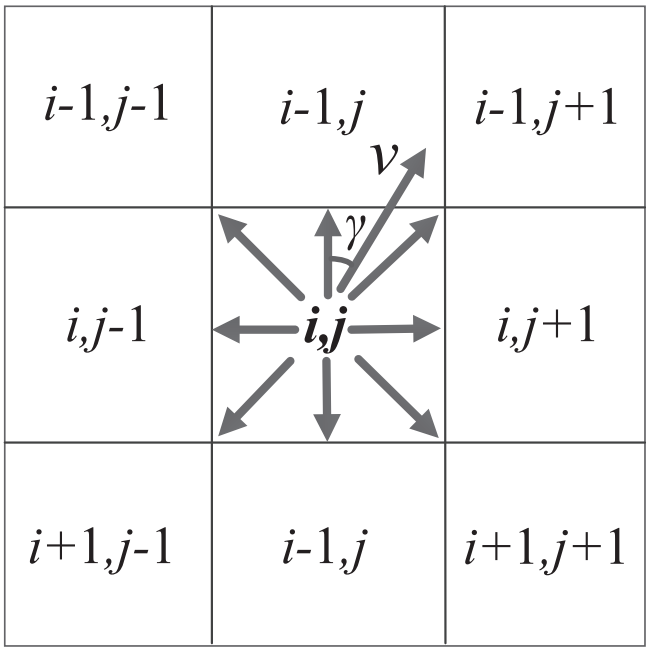

FIGURE 3 Schematic diagram of wildfire spread based on cellular automata.

The cell has the following five states: (i) $S = 0$ indicating unburned state, (ii) $S = 1$ indicating initial combustion (combustion completed but has not spread to the surrounding area), (iii) $S = 2$ indicating full combustion and has the ability to ignite surrounding cells, (iv) $S = 3$ shows that the wildfire has gradually extinguished, (v) $S = 4$ meaning that the wildfire has completely extinguished. After providing the fire information as input, the fully ignited cells will continue to ignite combustible cells in their neighbourhood, simulating the wildfire spread process. Traverse through all cell that has the potential to alter the combustion state. If a cell has $S = 0$, is combustible at the given time, and has combustible cells in its neighbourhood, calculate the state of that cell at the next instant using Equation (9); If $S = 1$ at this instant, the cell will transition to a fully ignited state in the next instant; If the cell's state is $S = 2$ but there are fully combustible cells or non-combustible regions in its neighbourhood, it will gradually extinguish; If the cell's state is $S = 3$ at this instant, then it becomes $S = 4$ in the next instant.

$$S_{i,j}^{t+1} = S_{i,j}^t + \frac{R_{i-1,j}^t + R_{i,j-1}^t + R_{i+1,j}^t + R_{i,j+1}^t}{a} + \frac{\left[\left(R_{i+1,j-1}^t\right)^2 + \left(R_{i-1,j+1}^t\right)^2 + \left(R_{i-1,j-1}^t\right)^2 + \left(R_{i+1,j+1}^t\right)^2\right]\Delta t^2}{2a^2} \tag{9}$$

where $d_{i,j}$ is the altitude of cell (i, j); $S_{i,j}^t$ is the cell (i, j) state at time t; a is the edge length of cell; Δt is time step, representing the time interval for updating the combustion status of the cell.

The schematic diagram of cellular automata is shown in Figure 3, where the spread speeds of wildfires in eight directions

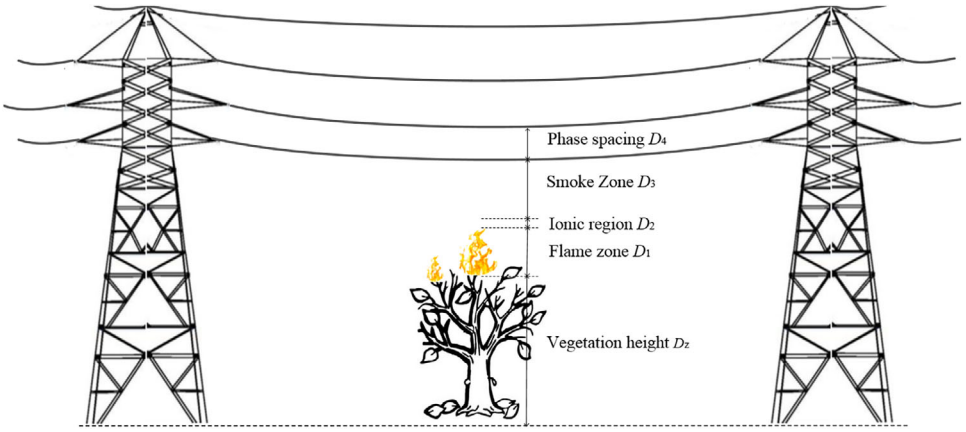

FIGURE 4 Zoning of air gap below transmission line during wildfire.

can be calculated as,

$$R_{i-1,j-1} = R_0 K_s K_{ze}^{0.1783 v_w \cos(315°-\gamma)} e^{3.533(-1)^G \left| \frac{d_{i-1,j-1}-d_{i,j}}{\sqrt{2}a} \right|^{1.2}} \quad (10)$$

$$R_{i-1,j} = R_0 K_s K_{ze}^{0.1783 v_w \cos\gamma} e^{3.533(-1)^G \left| \frac{d_{i-1,j}-d_{i,j}}{a} \right|^{1.2}} \quad (11)$$

$$R_{i-1,j+1} = R_0 K_s K_{ze}^{0.1783 v_w \cos(\gamma-45°)} e^{3.533(-1)^G \left| \frac{d_{i-1,j+1}-d_{i,j}}{\sqrt{2}a} \right|^{1.2}} \quad (12)$$

$$R_{i,j+1} = R_0 K_s K_{ze}^{0.1783 v_w \cos(\gamma-90°)} e^{3.533(-1)^G \left| \frac{d_{i,j+1}-d_{i,j}}{a} \right|^{1.2}} \quad (13)$$

$$R_{i+1,j+1} = R_0 K_s K_{ze}^{0.1783 v_w \cos(\gamma-315°)} e^{3.533(-1)^G \left| \frac{d_{i+1,j+1}-d_{i,j}}{\sqrt{2}a} \right|^{1.2}} \quad (14)$$

$$R_{i+1,j} = R_0 K_s K_{ze}^{0.1783 v_w \cos(180°-\gamma)} e^{3.533(-1)^G \left| \frac{d_{i+1,j}-d_{i,j}}{a} \right|^{1.2}} \quad (15)$$

$$R_{i+1,j-1} = R_0 K_s K_{ze}^{0.1783 v_w \cos(225°-\gamma)} e^{3.533(-1)^G \left| \frac{d_{i+1,j-1}-d_{i,j}}{\sqrt{2}a} \right|^{1.2}} \quad (16)$$

$$R_{i,j-1} = R_0 K_s K_{ze}^{0.1783 v_w \cos(\gamma+90°)} e^{3.533(-1)^G \left| \frac{d_{i,j-1}-d_{i,j}}{a} \right|^{1.2}} \quad (17)$$

2.3 | Tripping probability model of transmission line under the influence of wildfire

The historical cases of transmission line tripping show that it is possible to cause the transmission line tripping when the wildfire spreads below the transmission line. When the flame completely bridges the gap between the phase conductors or between the phase conductor and ground, the average withstanding electric field strength of the flame zone is 35 kV/m according to the breakdown test conducted. In this case, the gap breakdown voltage can be taken as the product of the flame withstand field strength and the gap distance. If the operating voltage exceeds the gap breakdown voltage, the tripping probability reaches 100%. When the flame partially bridges the gap, it is necessary to identify the gap's partitioning. Based on different breakdown mechanisms, the air gap below the transmission line is divided into three zones: (i) flame zone, (ii) ion zone and (iii) smoke zone, as illustrated in Figure 4. The breakdown voltage of each zone is calculated separately. High temperature in the flame zone leads to a decrease in air density and insulation performance. Many charges can gather in the ionic zone promoting the formation of flow injected discharge. The smoke zone occupies significant height below the transmission line, which distorts the electric field in the vicinity of the line through the soot particles, thus, promotes the breakdown [35].

There are two fault modes causing the transmission line tripout, namely, phase-to-ground breakdown and phase-to-phase breakdown. Further, it is necessary to calculate their tripping probabilities.

2.3.1 | Phase-to-ground breakdown

Faults in lines below 110 kV are mainly caused by phase-to-ground breakdown. As shown in Figure 4, the corrected phase-to-ground breakdown voltage during wildfire conditions is obtained by combining the electric field strengths of flame zone, ion zone and smoke zone. Under standard atmospheric conditions, the power frequency breakdown field strength, E_0 with an air gap of D (height of transmission line to ground) is,

$$E_0 = \begin{cases} 241.39, D < 4\text{m} \\ \dfrac{59D^2 + 1942D + 357.88}{D^2 + 3.89D}, D > 4\text{m} \end{cases} \quad (18)$$

1. Flame zone: The temperatures at the bottom and the end of the flame are about 950 and 300°C, respectively [36]. The breakdown electric field strength can be calculated as,

TABLE 2 Effective calorific values of different types of combustibles.

Combustible type	Lichen moss	Grass weed	Woody plant	Coniferous forest	Broad-leaved forest
H	8400–12,500	12,500–16,700	>16,700	20,900	16,700–20,900

TABLE 3 Correction factors for vegetation in ionic regions.

Vegetation type	Coniferous forest	Broad-leaved forest	Mixed forest	Shrub	Thatch grass
c	4	3	3.5	4	2

$$E_1 = E_0 \frac{T_a}{T_f} \tag{19}$$

$$T_f = T_a + 3.9 \frac{I^{2/3}}{D_{\tilde{\chi}}} e^{-\alpha(z-D_z)^2} \tag{20}$$

$$\alpha = \frac{1}{D_1 \left(D_1 + D_{\tilde{\chi}}\right)} \tag{21}$$

$$D_1 = \left(\frac{I}{273}\right)^{0.46} \tag{22}$$

$$I = HWR/600 \tag{23}$$

where T_a is the ambient temperature, K, T_f is the average temperature of the flame layer, K; D_1 is the height of the flame zone, m; α is the conversion coefficient of flame height; D_z is the vegetation height, m; I is the wildfire strength, kW/m; H is the effective calorific value of combustible materials, kJ/kg; R is the spread speed of wildfire, m/min.

The effective calorific values of different types of combustibles [37] are shown in Table 2.

Distinct models should be adopted when determining the effective combustible load for different vegetation types [38]. In substantial regions of southern China, the predominant afforestation tree species consist of Pinus massoniana and cedar. While they grow rapidly, their fire resistance is weak. Once they catch fire, crown fire may occur, which have the potential to escalate into massive forest fires. Pinus massoniana forest is dominated by middle-aged and young trees with medium canopy density. Canopy fires often occur in middle-aged and young forests of cedar [39]. The fuel loads of Pinus massoniana and cedar forests, excluding arbors (shrub layer, herb layer, litter etc.) are 16 and 12 t/hm^2 from experience, respectively.

Sunny slopes have strong sunlight, high temperatures, dry and flammable combustibles, causing most wildfires to occur. In this paper, it is assumed that the wildfires are located on sunny slopes. Further, slope also has a significant impact on the spread of wildfire. In general, the rate at which a wildfire expands increases with the slope. However, the shorter the fire residence time, the less harmful it is to trees. As a result, the spread of wildfire can be more intuitively simulated by choosing a slope between 10° and 30°. In this paper, a slope of 20° and an altitude of 200 m are considered. The relationship between diameter at breast height (DBH) and tree height of Pinus massoniana and cedar is discussed in [40].

The breakdown voltage in the flame zone is expressed as,

$$U_f = \int_{D_z}^{D_1+D_z} E_0 \frac{T_a}{T_f} d_z \tag{24}$$

2. Ionic zone: The breakdown field strength is,

$$E_2 = \frac{E_0}{1+c} \tag{25}$$

The breakdown voltage in the ion region is,

$$U_{\tilde{\chi}} = E_2 \cdot D_2 \tag{26}$$

where c is the correction factor for the breakdown field strength in case of vegetation, as shown in Table 3. The height of the ionic zone is D_2, usually taken as $0.1D_1$.

3. Smoke zone: Combustion-generated carbon particles are prone to bridge the gap when an electric field is present, and is calculated as,

$$E_3 = K_d K_h K_a \eta E_0 \tag{27}$$

$$K_d = \delta^n \tag{28}$$

$$\delta = \frac{\left(273 + q^0\right) p}{\left(273 + q*\right) p^0} \tag{29}$$

$$p \approx p^0 \tag{30}$$

$$q* = q^0 + \frac{3.9 I^{2/3}}{(D - D_z + D_1 + D_2)/2} \tag{31}$$

where p^0 and p are the atmospheric pressure under standard atmospheric conditions and wildfire conditions, kPa; q^0 and q^* represent the temperature under standard atmospheric conditions and the midpoint in the smoke zone, °C.

The air humidity correction factor can be expressed as,

$$K_h = h_c^w \tag{32}$$

where h_c is the humidity correction base; w is the humidity correction index.

The altitude correction factor can be expressed as,

$$K_a = \frac{1}{1.1 - 10^{-4} d} \tag{33}$$

where d is the altitude. When the altitude is less than 1000 m, the altitude correction factor is taken as 1. When the altitude is greater than 4000 m, it is temporarily impossible to accurately calculate.

The smoke concentration coefficient can be expressed as,

$$\eta = \frac{1}{14s + 1} \tag{34}$$

$$s = e^{-(D-D_1)^2/(2\sigma_D)} \tag{35}$$

where s is the smoke concentration, which can be taken as 0 to 100%. σ_D is the diffusion parameter of smoke in the direction D, which can be obtained through the diffusion parameter table.

The height of the smoke area is $D_3 = D - D_1 - D_2 - D_{\zeta}$. Therefore, the breakdown voltage, U_s can be expressed as,

$$U_s = E_3 \left(D - D_1 - D_2 - D_{\zeta}\right) \tag{36}$$

Combining the breakdown voltage of the flame zone, ion zone and smoke zone, the total breakdown voltage of air gap during wildfire conditions is,

$$U_g = U_f + U_z + U_s \tag{37}$$

2.3.2 | Phase-to-phase breakdown

The phase-to-phase breakdown occurs on transmission lines with rated voltages higher than 220 kV, accompanied by phase-to-ground breakdown. The phase-to-phase breakdown voltage during wildfire conditions is,

$$U_p = K_d' K_h' K_a \eta E_0 \tag{38}$$

The calculation methods for K_d' and K_b' are similar to those of the phase-to-ground breakdown case. The temperature of transmission line can be expressed as,

$$q' = q^0 + \frac{3.9 I^{2/3}}{D - D_{\zeta}} \tag{39}$$

2.3.3 | Calculation of comprehensive tripping probability

The transmission line tripping probability during wildfire can be calculated as,

$$p_{g,p} = \begin{cases} 0, & U \le 0.756 U_{g,p} \\ \dfrac{U - 0.756 U_{g,p}}{U_{g,p} - 0.756 U_{g,p}}, & 0.756 U_{g,p} < U < U_{g,p} \\ 1, & U \ge U_{g,p} \end{cases} \tag{40}$$

$$p_v = \begin{cases} p_g, & U_r < 220\ \text{kV} \\ 1 - \left(1 - p_g\right)\left(1 - p_p\right), & U_r \ge 220\ \text{kV} \end{cases} \tag{41}$$

where p_g is the probability of phase-to-ground fault; p_p is the probability of phase-to-phase fault; p_v is the probability of total breakdown; U_r is the rated voltage of transmission lines, kV.

2.4 | Resilience assessment model under wildfire disaster

Wildfire disasters significantly elevate the risk of large-scale power outages on transmission lines. A method for evaluating the resilience of transmission system considering the wildfire spread characteristics is proposed to improve the power grid's ability to respond to wildfire disasters.

When the transmission system is subjected to extreme wildfire disasters, numerous power equipment may shut down. To ensure the safety and security of the power system, necessary emergency measures such as load reduction will be ensured [41]. The whole response process of power system against wildfire disasters can be divided into the following four stages: (i) preparation and prevention, (ii) resistance and absorption, (iii) response and adaptation, and (iv) recovery, as shown in Figure 5.

The transmission lines begin to malfunction when wildfire disaster occur at time t_0, and the system is forced to curtail load at t_1, until the load decreases to a lower level at t_2. The load is maintained at a low level between t_2 and t_3, and the system remains stable. As the maintenance personnel repair the faulty lines, the system performance gradually recovers at t_3. The effect of wildfire disasters on the transmission system has completed at t_4; the load on the system does not return to its initial level until t_5.

In this paper, the missing area of the system load curve during extreme wildfire disasters is utilized as a metric to assess the transmission system's resilience. The missing area takes into account both the load loss experienced during disasters and the time required for the system to return to normal operation.

$$\mathrm{AR} = E\left[\frac{\int_{t_0}^{t_4} L(t)\mathrm{d}t}{\int_{t_0}^{t_4} TL(t)\mathrm{d}t}\right] = \sum_{k=1}^{k_n} p_k \left[\frac{\int_{t_0}^{t_4} L(t)\mathrm{d}t}{\int_{t_0}^{t_4} TL(t)\mathrm{d}t}\right] \tag{42}$$

where $E(\cdot)$ represents the expected value; p_k is the occurring probability of scenario k; k_n is the total number of scenarios; $L(t)$ is the actual load curve of the system subjected to a wildfire disaster; $TL(t)$ is the normal load curve of the system without faults; AR refers to the resilience of the power transmission during wildfire disasters.

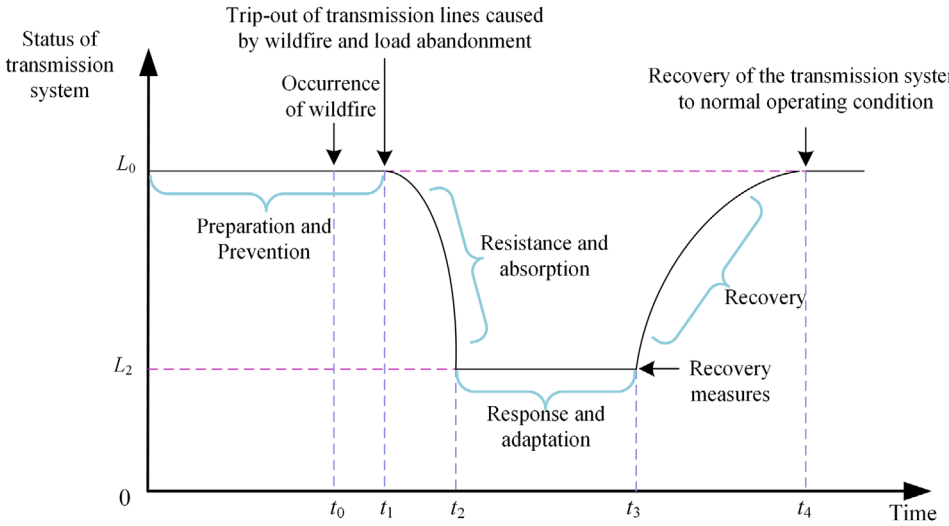

FIGURE 5 The whole response process of power system against wildfire disasters.

The main steps of resilience assessment are as follows:

1. Location of the fire point, vegetation information, and transmission line parameters are to be provided as inputs. Calculate the tripping probability for each line and obtain typical fault scenarios.
2. Location of fault on the line in typical fault scenarios is provided as input to the component repair model. Optimal repair time in each scenario and the line state during repair process are obtained and provided as inputs to the transmission response model.
3. Determine the optimal load reduction in each fault scenario based on the simulation studies.
4. After eliminating all faults in the system, the resilience index of the system is calculated according to Equation (42).

2.4.1 | Fault scenario generation for transmission system caused by wildfire disasters

It is crucial to select the fault scenarios involving wildfire for the transmission system's resilience assessment. Since there are several transmission lines and possible fault scenarios, it is necessary to select a typical fault scenario under extreme wildfire conditions to evaluate the transmission system's resilience [42].

Considering the scale of calculations and the applicability of the model, the non-sequential Monte Carlo simulation method is chosen to sample the states of power system components during wildfire disasters and generate possible fault scenarios. Finally, the information entropy method is implemented for screening the fault scenarios. The state of the system can be determined using the non-sequential Monte Carlo simulation method and the fault probability of the elements in a given state can be sampled to derive the state of the elements in the system. The component has two states during the extreme disaster event: (i) normal state and (ii) outage state. Say, $X_l(t)$ is the state of transmission line l at time t. If $X_l(t) = 1$, the transmission line l is in outage state. Similarly, if $X_l(t) = 0$, the transmission line l is in normal state. $X_l(t)$ is obtained by comparing the component failure probability, $p_{l,t}$ with the random number rand_m which obeys the uniform distribution $U(0,1)$.

$$X_l(t) = \begin{cases} 1, p_{l,t} > \text{rand}_m \\ 0, p_{l,t} \le \text{rand}_m \end{cases} \tag{43}$$

where $X_l(t)$ is the state of component m at time t; rand_m is a random number; $p_{l,t}$ is the failure probability of component l.

The characteristic of Monte Carlo method is that as the simulated sampling time increases, the result approach the actual value. The information entropy proposed by Shannon can eliminate the redundancy of known information [43], by obtaining the average of remaining important information and quantifying the uncertain variables. Therefore, the information entropy for different scenarios during a single wildfire disaster event is obtained by using the information entropy method to screen the fault scenarios. The information entropy can be expressed as,

$$\zeta = \sum_{l \in B} \left(-\log_2 p_{l,t}\right) z_{l,t} \tag{44}$$

where $p_{l,t}$ is the failure probability of component l at time t; ξ is the information entropy; B is the transmission network line set; $z_{l,t}$ represents the fault indicator of line l at time t. When a fault occurs, $z_{l,t}$ is 0 during normal operation.

The system information entropy value of the selected typical fault scenario should meet the following requirement:

$$W_{\min} \le \sum_{l \in \boldsymbol{B}} (-\log_2 p_{l,t}) z_{l,t} \le W_{\max} \tag{45}$$

where, $W_{\min}$ and $W_{\max}$ are the minimum and maximum system information entropy in the selected fault scenario, respectively.

2.4.2 | Response model for transmission system during wildfire disasters

To ensure the safety of the system, it is necessary to reschedule the generators or balance the supply and demand of the transmission network through load curtailment. The optimal power flow model based on DC power flow is commonly used for fast calculation in risk assessment of transmission systems. This paper establishes an optimal power flow model with the goal of minimizing the amount of load reduction. The objective function of the transmission network's disaster response can be expressed as [44],

$$\min \sum_{t=1}^{t} \sum_{j=1}^{N_D} P_{j,t}^{cur} \tag{46}$$

where $P_{j,t}^{\mathrm{cur}}$ is the load reduction of node j at time t; N_D is the number of nodes with load.

The constraints of generator and load power balance, output maximum and minimum limits, and load curtailment can be expressed as,

$$\sum_{i=1}^{N_G} P_{i,t}^{\mathrm{G}} = \sum_{j=1}^{N_D} \left(P_{j,t}^{\mathrm{L}} - P_{j,t}^{cur} \right) \tag{47}$$

$$0 \le P_{i,t}^{\mathrm{G}} \le P_{i,\max}^{\mathrm{G}} \tag{48}$$

$$0 \le P_{j,t}^{cur} \le P_{j,t}^{\mathrm{L}} \tag{49}$$

where $P_{i,t}^{\mathrm{G}}$ is the output active power of ith generator unit during time t; $P_{j,t}^{L}$ is the load demand of jth node at time t; $P_{i,\max}^{\mathrm{G}}$ is the upper limit of output active power of ith generator unit; N_{G} is the number of nodes of the generator.

The power flow equation and constraints of the line are expressed as,

$$F_l = (\theta_{l,t}^{\mathrm{fr}} - \theta_{l,t}^{\mathrm{to}}) / x_l \tag{50}$$

$$-f_{l,\max} \cdot \left(1 - z_{l,t}\right) \le F_l \le f_{l,\max} \cdot \left(1 - z_{l,t}\right) \tag{51}$$

where F_l is the active power flow for transmission line l; $\theta_{l,t}^{\mathrm{fr}}$ and $\theta_{l,t}^{\mathrm{to}}$ are the voltage phase angle of the first and end nodes of line l, respectively; F_l and $f_{l,\max}$ are the active power flow and active power flow limits for line l, respectively.

2.4.3 | Post-disaster recovery model for transmission system

In the post-fire recovery stage, the maintenance team will follow a predetermined route to reach the fault line, quickly extinguish the fire around the line, repair all the faults, and return to the maintenance centre. Due to the large span area of the transmission system, the time the maintenance team spends travelling cannot be disregarded; therefore, the component repair time is considered as the sum of the journey time and the maintenance time.

The goal of the model is to minimize the total repair time of all faulty lines as,

$$\min \sum_{r \in N \backslash \{0\}} \tau_r \tag{52}$$

where τ_r is the repair time of faulty component r; N is the faulty lines set.

Assuming that the maintenance team set is C and the fault line set is N, binary variables are used to define the maintenance situation of the team. The value of the binary variable is 1 when the maintenance team c passes the fault variable r and it is 0 otherwise. All fault lines only need to be repaired once during the maintenance process. After completing all maintenance tasks, the maintenance team c must return to the maintenance center from where they started. This constraint can be expressed as,

$$\sum_{c \in C} \sum_{r \in N \backslash \{0\}} x_{0,r,c} = \sum_{c \in C} \sum_{r \in N \backslash \{0\}} x_{r,0,c} = n^{\mathrm{crew}} \tag{53}$$

where C is the maintenance team set; $x_{0,r,c}$ and $x_{r,0,c}$ are all decision variables for scheduling paths, representing the departure and return of maintenance teams from the maintenance center; n^{crew} represents the number of maintenance teams.

After repairing a line, maintenance team c will go to the next faulty line based on the following criteria.

$$\sum_{s \in N \backslash \{r\}} x_{r,s,c} - \sum_{s \in N \backslash \{r\}} x_{s,r,c} = 0, r \in N \tag{54}$$

where $x_{r,s,c}$ and $x_{s,r,c}$ are all decision indicators for the scheduling path of maintenance personnel, representing the departure and return of maintenance team c from point r to point s.

The time for the maintenance team c to arrive at the next fault line s meets,

$$t_{r,c} - t_{s,c} + t_r + t_{r,s,c}^{rou} \le M \left(1 - x_{r,s,c}\right) \tag{55}$$

$$\begin{cases} 0 \le t_{r,c} \le M \cdot y_{r,c}, r \in N \backslash \{0\} \\ t_{r,c} = t_i, r \in \{0\} \end{cases} \tag{56}$$

where $t_{r,c}$ is the time when maintenance team c arrives at faulty line r; $t_{s,c}$ is the time when maintenance team c arrives at faulty line s; t_r is the time required for repair team to repair faulty component r;$t_{r,s,c}^{\mathrm{rou}}$ is the time for maintenance team c to travel from point r to point s; M is a big enough positive number; t_i is the time to prepare the overhaul team for departure.

When the fault line r is repaired, its status is set as 1, otherwise it is 0. The maintenance time of the fault line r meets,

$$\tau_r \ge \sum_{c \in C} \left(t_{r,c} + t_r y_{r,c} \right), r \in N \backslash \{0\} \tag{57}$$

$$\sum_{c \in C} y_{r,c} = 1, r \in N \backslash \{0\} \tag{58}$$

$$\tau_r \le \sum t \cdot h_{r,t} \le \tau_r + 1 - \varepsilon, r \in F \backslash \{0\} \tag{59}$$

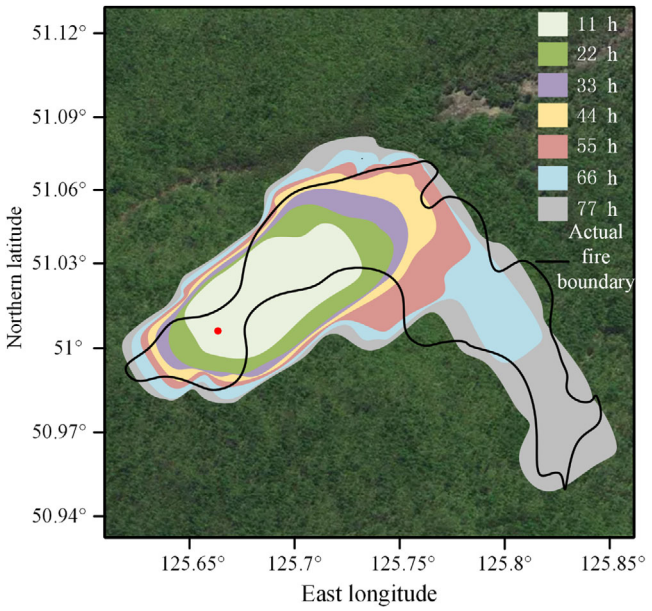

FIGURE 6 Simulated results of time sequence map of wildfire spread and comparison with actual final wildfire.

where $y_{r,c}$ is the binary variable whether maintenance team c passes through the line r; $h_{r,t}$ is the component repair completed binary coefficient; ε is any small real number.

Assuming that there is only one maintenance crew overall for the purposes of this paper,

$$n^{\text{crew}} = 1 \tag{60}$$

3 | RESULTS AND DISCUSSION

3.1 | Results of wildfire spread

3.1.1 | Accuracy verification

In order to verify the accuracy of the model constructed in this paper, a case of meadow forest fire caused by outdoor smoking in the Daxinganling of Heilongjiang Province on April 30th [45] was selected for comparative analysis. After 77 h of emergency fighting, the fire was successfully brought under control on May 3rd. This paper subdivided the fire into seven time periods, each time period was 11 h. The coordinate of fire point is longitude 125.675° east, latitude 51.009167° north. The size of the fire site was 20 km×20 km and the side length of cell is 100 m, as shown in Figure 6. The black curve is the actual boundary of the fire site. Due to the harsh environment of the fire site at that time and the limitation of monitoring means, it is difficult to output the size of the fire site in real time. Therefore, only the actual area of the final fire site was compared with the simulated result of the proposed wildfire spread model. As can be seen from Figure 6, the proposed model shows high accuracy in predicting the trend of wildfire spread.

TABLE 4 Transmission line wildfire warning threshold.

$L_{\min}$	Alarm level
$L_{\min} \le 500$ m	Level 1
$500 < L_{\min} \le 1000$ m	Level 2
$1000 < L_{\min} \le 3000$ m	Level 3

3.1.2 | Results of wildfire spread in specific scene

For the simulation studies, it is assumed that the spread time is 100 min, step length is 0.5 min, temperature is 20°C, air humidity is 70%, and fuel water content is 10%. The spread of wildfires is simulated in flat and real scenarios.

The vegetation type is set to fir tree and K_s is 0.8. The spread results for 100 and 200 min without wind and in flat conditions are simulated. The spread characteristics of wildfires with the south wind and the west slope are also simulated and the results are shown in Figure 7.

It can be seen from Figure 7 that as the wind speed and slope increase, the propagation speed of the downwind and uphill case increases, while the propagation speed of the upwind and downhill case decreases. The fire site's area grows as wind speed and slope rise, and it progressively shifts from a circular to a flatter shape.

3.1.3 | Analysis results of actual scenarios

A 500 m by 500 m area in Gushan, with longitude and latitude ranging from (119.43735, 26.09186) to (119.442348, 26.087374), has been chosen to serve as the experimental area. Mixed forest type of vegetation is considered with an average height of 8 m, a daily relative minimum humidity of 70%, and a wind speed of 3 m/s in southern direction. There is a transmission line in the northeast direction The real-time alarm levels of the transmission line are shown in Table 4. The topographic map of Gushan is shown in Figure 8, while the spread map is shown in Figure 9.

3.2 | Calculation results of tripping probability of transmission line

3.2.1 | Model accuracy verification

To verify the accuracy of the proposed transmission line tripping probability model proposed in this paper, three representative fire points were selected from the transmission panoramic monitoring platform of a province in China to calculate the tripping probability, and compared with actual fire scene information, as shown in the Table 5. The results indicate that the predicted tripping probability is consistent with the actual occurrences of wildfires near the transmission line.

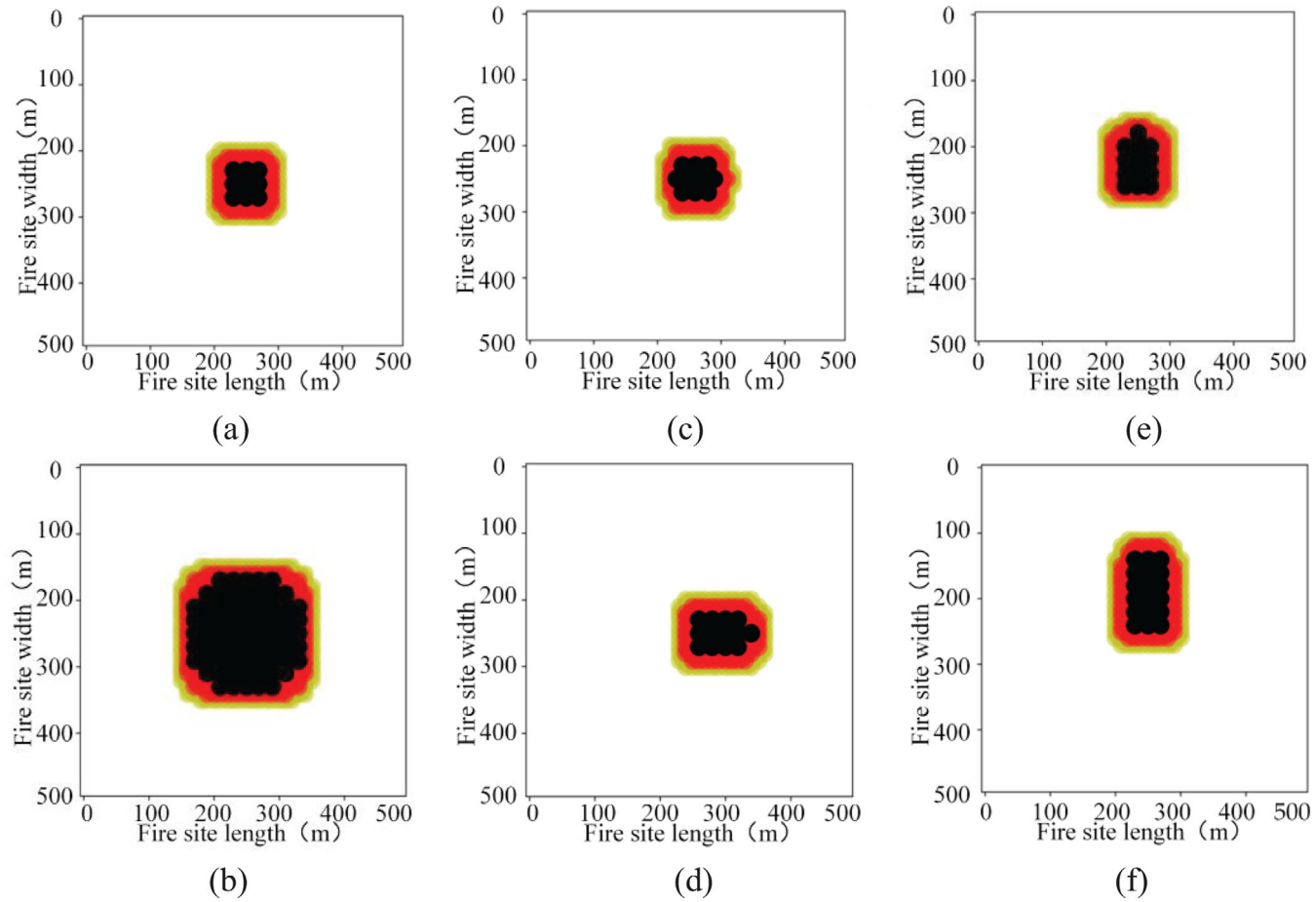

FIGURE 7 Results of wildfire spread under different conditions, (a) 100 min, calm, flat, (b) 200 min, calm, flat, (c) 100 min, calm, tanφ = 0.1, (d) 100 min, calm, tanφ = 0.3, (e) 100 min, flat, v_w = 3 m/s, (f) 100 min, flat, v_w = 6 m/s.

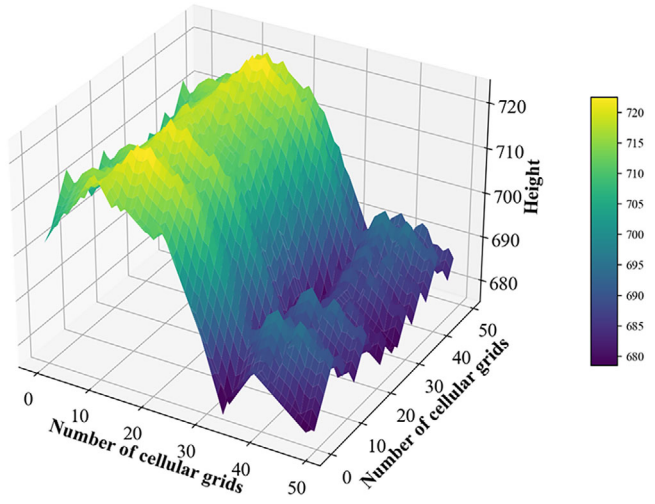

FIGURE 8 Topographic map of Gushan.

3.2.2 | Example analysis

The probability of tripping the transmission line is computed when the wildfire spreads beneath it. The calculation example shown in Section 3.1 is used for analysis, while assuming that the smoke and dust concentration is 25%, the absolute humidity is 11 g/m^3, and clear weather with no terrain obstacles between the fire point and the line. The breakdown voltage is corrected considering the coefficient correction formula. Further, the breakdown probabilities between phase and ground, and between phase and phase for each voltage level are calculated using the aforementioned method, and the results are presented in Tables 6 and 7.

Considering that vegetation height is more easily obtained than other variables, and has certain impact on factors such as wildfire spread, flame height, temperature and humidity, and pressure. Therefore, Pinus massoniana and cedar that are common in Fujian are considered to predict the tripping probability of transmission lines under different vegetation heights, as shown in Figures 10 and 11. The results presented in these figures reflect the relationship between the outage probabilities for two types of faults on the overhead transmission lines and vegetation height under two types of vegetation. The probability of both types of faults continuously increases with the increase in vegetation height. The height of vegetation has a linear relationship with the probability of phase-to-ground breakdown, and in a particular community, this relationship rapidly increases with an increase in vegetation height, posing a significant risk.

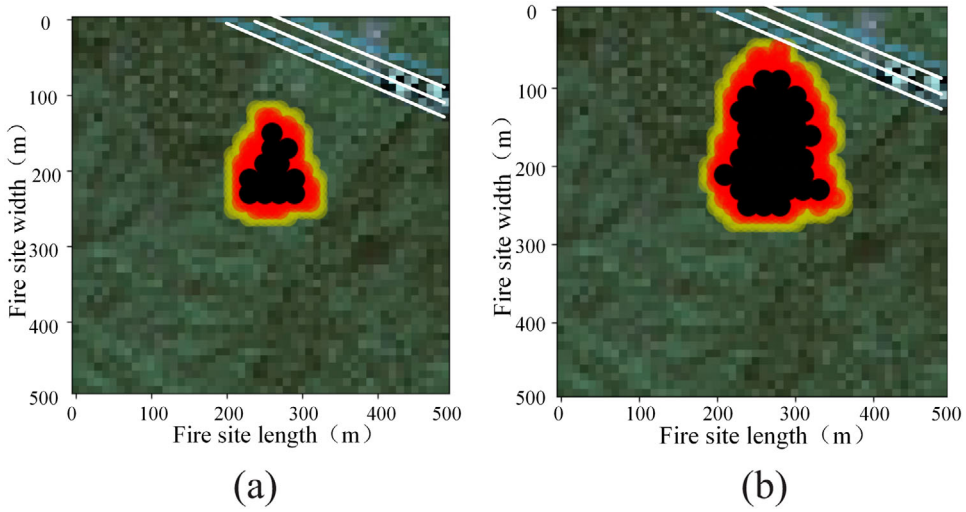

FIGURE 9 Results of fire spread below the transmission line. (a) 60 min. (b) 87.5 min.

TABLE 5 Model accuracy verification.

Line No.	Voltage level (kV)	Main vegetation type	Predicted tripping probability	Effect of the wildfire on the transmission line
1	220	Cedar	97.98%	The warning message was not received in time. The wildfire spread below the transmission line and caused a tripping accident.
2	220	Cedar	84.71%	The shortest distance between the wildfire and the transmission line was 50 m when the warning message was received, and the reclosing was exited in advance. The staff extinguished the wildfire in time and prevented the transmission line from tripping.
3	110	Marshy grassland	3.67%	The shortest distance between the wildfire and the transmission line was greater than 200 m when the warning message was received. There was a river between the wildfire and the transmission line, so the wildfire had little effect on the transmission line.

TABLE 6 Probability of phase-to-ground breakdown of conductors at different voltage levels.

Voltage level (kV)	110	220	500
Height of conductor to ground (m)	11.5	14	35
Probability of phase-to-ground breakdown	0	0.8559	0.4424

TABLE 7 Probability of phase-to-phase breakdown at different voltage levels.

Voltage level (kV)	110	220	500
Interphase distance (m)	4.25	8	17
Probability of phase-to-ground breakdown	—	0.165728	0

From the study of two vegetation types, it can be found that phase-to-ground breakdown is more common compared to phase-to-phase breakdown. When evaluating the impact of vegetation height on trip probability, the transmission line's fault state can be roughly judged using phase-to-ground faults to minimize computational burden.

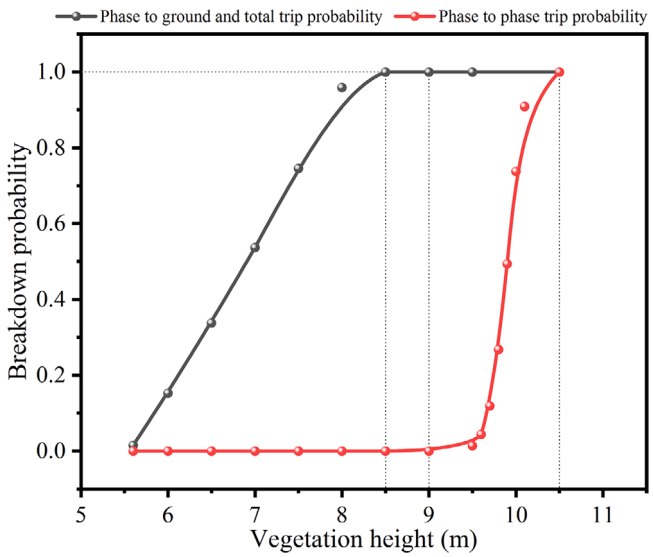

FIGURE 10 Variations in trip probability of overhead transmission line with *Pinus massoniana*'s height.

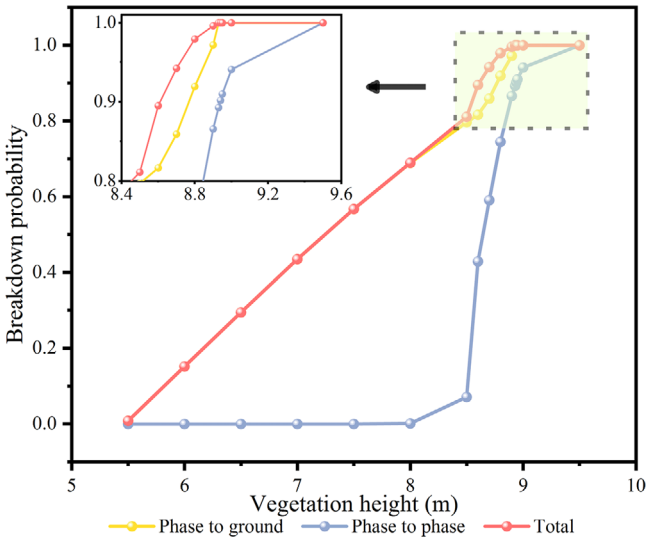

FIGURE 11 Variations in trip probability of overhead transmission line with cedar's height.

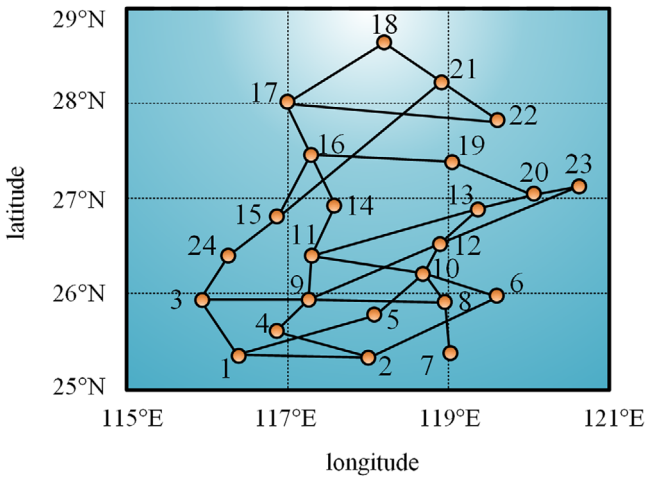

FIGURE 12 Geographical location of IEEE RTS-79 system in Fujian province.

3.3 | Results of resilience assessment of transmission lines during wildfire conditions

3.3.1 | Fault scenario generation

In this article, IEEE RTS-79 system is considered as an example, which consists of 24 nodes and 34 lines. The system parameters are detailed in [46], while the fire point information is detailed in [36]. The longitude and latitude of each node in the system is shown in Figure 12.

The node system data and fire point information are imported to obtain the vegetation height and trip probability of 34 lines in the system, as shown in Figure 13.

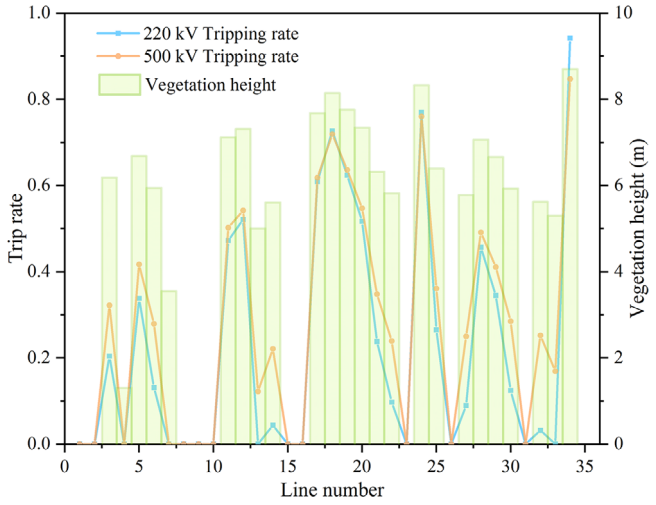

FIGURE 13 Vegetation height and transmission line's tripping probability with two voltage levels.

3.3.2 | Screening of typical fault scenarios

Based on Monte Carlo sampling, the tripping probability of a single transmission line during wildfires is used to select possible fault scenarios.

The fault scenarios are generated based on the line failure rate calculated in Section 2.3, and the system entropy corresponding to each scenario can be calculated by combining the fault lines in different fault scenarios with Equation (44). Then the probability distribution of each fault scenario corresponds to the respective system entropy distribution. The magnitude of entropy is related to the characteristics of the system. The higher the probability of entropy, the greater the probability of the corresponding scene appearing in the wildfire disaster. In this paper, the scenario with entropy between 11 and 15 is selected as a typical fault scenario.

To streamline the selection process, 20 typical fault scenarios with 6–8 faults are selected for analysis. The influence of load change and improvement measures on the system resilience of each scenario is analysed by controlling a single variable.

3.3.3 | Resilience assessment results

Considering a team of maintenance personnel, the time required to repair each line is 2 h. Say, the wildfire disaster is detected at 1 o'clock and the step size is set to 1 h, the following four scenarios are discussed using the CPLEX solver in MATLAB:

Case 1: Line voltage of the system is 220 kV.
Case 2: Line voltage of the system is 500 kV.
Case 3: Based on Case 1, lines 19, 25, and 34 with high tripping probability are cut off before the wildfire, while the loads on these lines are connected to the standby line. Loads are connected back to the original lines after the disaster.

TABLE 8 Resilience assessment of electric power transmission system under four conditions.

Case	Case 1	Case 2	Case 3	Case 4
AR	0.8561	0.8328	0.8903	0.8713

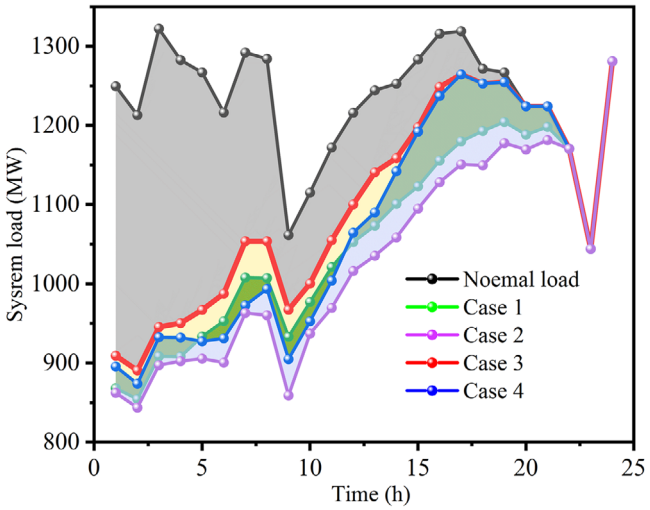

FIGURE 14 24-h load curve during the four cases.

Case 4: Based on Case 2, lines 19, 25, and 34 with high tripping probability are cut off before the wildfire, while the loads on these lines are connected to the standby line. Loads are connected back to the original lines after the disaster.

The simulation results are shown in Table 8 and Figure 14.

From Figure 13, it can be concluded that the system has undergone a large-scale load curtailment at the beginning of first hour. In case 2, the 500 kV line has the largest load curtailment of 383.95 MW, while the 220 kV line has slightly lower load curtailment of 376.54 MW in Case 1. This indicates that under the same circumstances, the 500 kV line was more severely affected by wildfires. Strengthening the lines with a high probability of failure enhances their anti-interference ability and prevents them from tripping due to wildfire disasters as evident from cases 3 and 4. In case 3, the load curtailment was reduced to 338.63 MW. The load was restored to 37.91 MW compared to case 1 before the reinforcement. While the required recovery time was also less than case 1, the initial state was restored after 20 h. According to the results presented in Table 7, the repair measures proposed in this article can effectively improve the system's resilience but only for systems with dual-circuit power supply. At present, high-cost measures such as installing isolation belts, pruning the vegetation along the line and improving the efficiency of system restoration are being used to improve the system's resilience for systems without dual-circuit power supply.

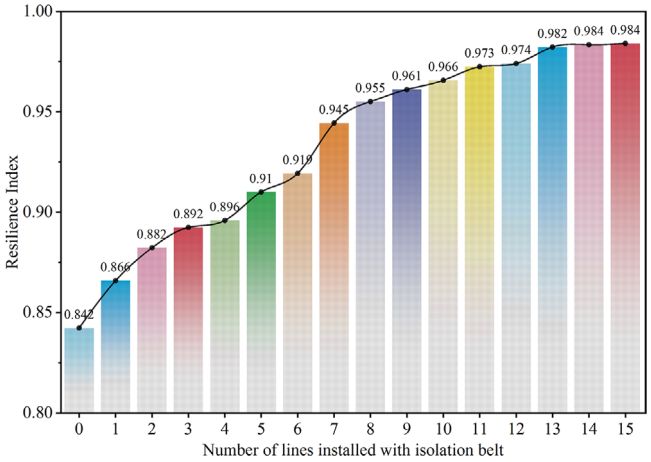

FIGURE 15 Resilience index of different numbers of spacers.

3.4 | Resilience enhancement measures

3.4.1 | Additional isolation belt

The isolation belt around the transmission lines can effectively protect the line from wildfires, but it is too expensive to install the isolation belt on all the lines. Therefore, lines with higher tripping probability must be selected for installing the isolation belts. The relationship between the system's elastic index and the number of isolators installed on the line is shown in Figure 15 (taking the 220 kV line as an example).

It can be seen from Figure 14 that the resilience index of the system is 0.8422 when the isolation belt is not installed. The resilience index grows at its highest rate when there are seven isolation belts; after that, it begins to slow down and eventually approaches 1. Thus, considering the expenses and the proper installation of the isolation belt, the system offers some flexibility to improve the assistance.

3.4.2 | Trim the vegetation along the line

In addition to installing the isolation strips along the transmission line, it is also possible to prevent the wildfires by pruning vegetation. The system's resilience index increases with the amount of vegetation that is pruned, as does the probability of a transmission line wildfire tripping. Based on this, the relationship between resilience indicators and the percentage of vegetation pruned is explored. Here, the pruning coefficient, e_1 is introduced to represent the percentage of vegetation pruned. The relationship between trimmed vegetation height and conventional vegetation height is given in Equation (61). The relationship between system's resilience and vegetation pruning coefficient is shown in Figure 16.

$$D_{Nc} = (1 - e_1) \times D_c \tag{61}$$

where D_{Nc} is the trimmed vegetation height; D_c is the origin vegetation height; e_1 is pruning coefficient.

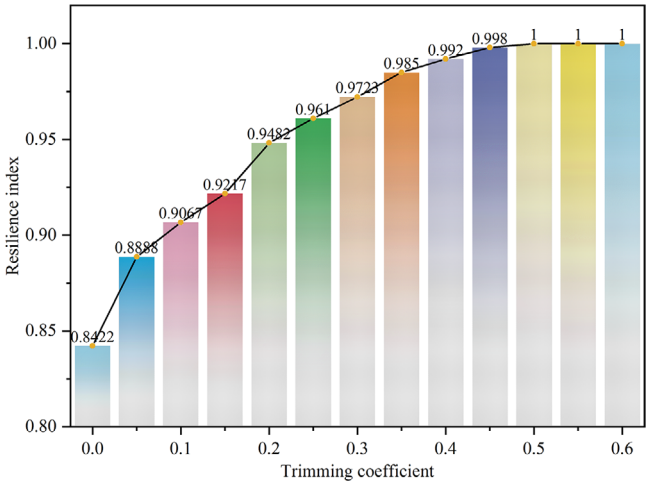

FIGURE 16 Resilience indicators with different pruning coefficients.

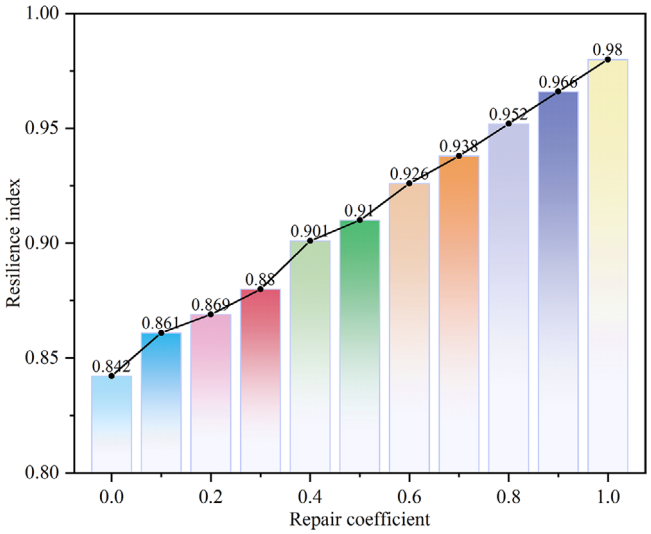

FIGURE 17 Resilience index values under different repair coefficients.

From Figure 16, it can be seen that the system's resilience increases with an increase in vegetation pruning coefficient, showing a trend of first quick, then slow. When the construction coefficient is 0.05, the increase in resilience index is the largest. When the trimming coefficient is 0.5, the system resilience reaches 1. At this point, the transmission line is unlikely to experience a trip incident due to wildfire, and the system can withstand wildfire disasters to the maximum extent possible.

3.4.3 | Improve the efficiency of system restoration

The restoration efficiency of the system is inversely proportional to its recovery time. The quality of various maintenance teams corresponds to different restoration efficiency. Maintenance efficiency can be improved by recognizing the fault types and locations quickly, strengthening professional training, improving maintenance equipment, and improving driving tools. The system is more resilient and needs less recovery time when its components repair team operates more efficiently. In this article, the repair time of faulty lines under conventional configuration is set to 2 h, and the relationship between system resilience and the percentage reduction in repair time is explored. Here, the repair coefficient, e_2 is introduced to represent the percentage reduction in repair time. The relationship between the repair time after improving the efficiency and the repair time under conventional configuration is given by Equation (62). Similarly, the relationship between system resilience and repair coefficient is shown in Figure 17.

$$t_{\mathrm{Nc}} = (1 - e_2) \times t_{\mathrm{c}} \tag{62}$$

where, t_{Nc} is repair time after improving efficiency; t_{c} is repair time under conventional configuration; e_2 is repair coefficient.

As shown in Figure 17, there is a positive correlation between the resilience index and maintenance efficiency. When the repair coefficient is 1, the resilience index approaches 1. However, due to the time taken for the maintenance team to reach the faulty line and the ideal state at this time, the resilience index cannot reach 1.

4 | CONCLUSIONS

This article uses Python as a platform to accurately anticipate the spread process of wildfire. It is based on the Wang Zhengfei model and combines the features of cellular automata and wildfire. The time when wildfire spreads below the transmission line is calculated, and the trip probability of the transmission line is obtained. Finally, the IEEE RTS-79 system was simulated using the CPLEX solver to analyse the effectiveness of various resilience improvement measures in responding to wildfire disasters. The following conclusions were drawn:

1. In the mixed forest with cedar and Pinus massoniana, the speed and spread area of fire have gradually increased with the increase of downwind speed and uphill slope. The fire began to spread below the transmission line 87.5 min after it began, and it grew over time. It is necessary to control the fire as soon as possible, and within 1 h is the best.
2. When the wildfire spreads beneath a transmission line, the lines may trip. As the vegetation height below the transmission line increases, the probability of phase-to-ground fault and phase-to-phase fault will increase. In the same calculation example, the probability of phase-to-ground fault occurring is higher than that of phase-to-phase fault, which can serve as a benchmark for judging the trip of the transmission line.
3. The effect of enabling backup lines, installing isolation strips, pruning vegetation along transmission lines, and improving restoration efficiency on system resilience was analysed using IEEE RTS-79 system. The simulation results show that the above resilience improvement measures can effectively improve the system resilience.

This article simulates the wildfire spread trends under different slopes and wind speeds to predict the spread area of wildfire, which can act as a technical support for quickly predicting the developments in trends of wildfire. The probability models of wildfire faults proposed in this article can be applied as transmission line wildfire warning system. The resilience assessment method can quantitatively analyze the improvement effect of various resilience improvement measures, providing a reference for formulating an optimal resilience improvement decision. This has a significant impact in reducing the loss of transmission lines during wildfires.

AUTHOR CONTRIBUTIONS

Shengwen Shu: Conceptualization; funding acquisition; project administration; supervision; writing—review & editing. **Nan Xiao**: Investigation; software; visualization; writing—original draft. **Shiyun Cao**: Data curation; formal analysis; methodology; writing—original draft. **Jun Xu**: Resources; validation. **Chaoying Fang**: Software; visualization. **Wenbing Xie**: Data curation; formal analysis.

ACKNOWLEDGEMENTS

This work was supported by the National Natural Science Foundation of China (52207150).

CONFLICT OF INTEREST STATEMENT

The authors declare no conflicts of interest.

DATA AVAILABILITY STATEMENT

The data that support the findings of this study are available on request from the corresponding author.

ORCID

Shengwen Shu https://orcid.org/0000-0003-0181-9563

REFERENCES

1. Wu, T., Hu, Y., Ruan, J., et al.: Air gap breakdown mechanism of model AC transmission line under forest fires. High Volt. Eng. 37(5), 1115–1122 (2011)
2. Zhou, E., Huang, Y., Chen, J., et al.: Graph theory based fire risk prediction level model of overhead transmission lines. South. Power Syst. Technol. 14(4), 8–16 (2020)
3. Wang, Y., Deng, H., Wang, X., et al.: Optimal configuration and operation strategy of mobile energy storage in distribution network considering spatial-temporal evolution of typhoon. Autom. Electr. Power Syst. 46(9), 42–51 (2022)
4. Tang, W., Yang, Y., Li, Y., et al.: Investigation on resilience assessment and enhancement for power transmission systems under extreme meteorological disasters. Proc. CSEE 40(7), 1–12 (2020)
5. Liang, Y., Zhou, L, Chen, J. et al.: Monitoring and risk assessment of wildfires in the corridors of high-voltage transmission lines. IEEE Access 8, 170057–170069 (2020)
6. Lin, Z., Liu, H, Wotton, M.: Kalman filter-based large-scale wildfire monitoring with a system of UAVs. IEEE Trans. Ind. Electron. 66(1), 606–615 (2019)
7. Wang, Z., Ding, T., Li, L., et al.: Policies and measures of public safety power shutoff for enhancing grid resilience under catastrophic wildfire in California state of America. Electr. Power Autom. Equip. 42(03), 36–44 (2022)
8. Yang, R, Yang L.: Resilience assessment and improvement for electric power transmission systems against typhoon disasters: a data-model hybrid driven approach. Energy Rep. 8, 10923–10936 (2022)
9. Zhao, N.: Full-time scale resilience enhancement framework for power transmission system under ice disasters. Int. J. Electr. Power Energy Syst. 126, 106609 (2021)
10. Muhs, W., John W. Parvania, M., et al.: Characterizing probability of wildfire ignition caused by power distribution lines. IEEE Trans. Power Delivery 36(6), 3681–3688 (2020)
11. Souto, L., Yip, J., Wu, W., et al.: Power system resilience to floods: modeling, impact assessment, and mid-term mitigation strategies. Int. J. Electr. Power Energy Syst. 135, 107545 (2022)
12. Lian, A., Qian, T., Li, Z., et al.: Resilience assessment for power system based on cascading failure graph under disturbances caused by extreme weather events. Int. J. Electr. Power Energy Syst. 145, 108616 (2023)
13. Dehghani, F., Mohammad, M., Mazaher, K.: Age-dependent resilience assessment and quantification of distribution systems under extreme weather events. Int. J. Electr. Power Energy Syst. 150, 109089 (2023)
14. Liu, J., Li T., Meng Y., et al.: Probabilistic framework for seismic resilience assessment of transmission tower-line systems subjected to mainshock-aftershock sequences. Reliab. Eng. Syst. Saf. 242, 109755 (2024)
15. Perera, A., Zhao, B., Wang, Z., et al.: Optimal design of microgrids to improve wildfire resilience for vulnerable communities at the wildland-urban interface. Appl. Energy 335, 120744 (2023)
16. Serrano, A., Liao, Z., Li, H., et al.: A novel resilience assessment for active distribution networks including a DER voltage regulation scheme considering windstorms. Int. J. Electr. Power Energy Syst. 153, 109310 (2023)
17. Yang, W., Sparrow, S., Ashtine, M., et al.: Resilient by design: preventing wildfires and blackouts with microgrids. Appl. Energy 313, 118793 (2022)
18. Trakas, D., Hatziargyriou, N.: Optimal distribution system operation for enhancing resilience against wildfires. IEEE Trans. Power Syst. 33(2), 2260–2271 (2017)
19. Sayarshad, H. R.: Preignition risk mitigation model for analysis of wildfires caused by electrical power conductors. Int. J. Electr. Power Energy Syst. 153, 109353 (2023)
20. Rothermel, C.: A mathematical model for predicting fire spread in wildland fuels. Intermt. For. Range Exp. Stn. 115, 1–41 (1972)
21. Perry, G.: Current approaches to modelling the spread of wildland fire are view. Prog. Phys. Geog. 22, 222–245 (1998)
22. McArthur, A.: Fire behavior in eucalypt forests Canberra. For. Timber 12, 1–36 (1967)
23. Wang, Z.: The measurement method of the wildfire initial spread rate. J. Mt. Res. 1(2), 42–51 (1983)
24. Pu, Z., Ruan, J., Wu, T., et al.: Influence of particles in flame on the characteristics of gap discharge. High Volt. Eng. 40(1), 103–110 (2014)
25. Huang, D., Li, P., Ruan, J., et al.: Review on discharge mechanism and breakdown characteristics of transmission line gap under forest fire condition. High Volt. Eng. 41(2), 622–632 (2015)
26. Robledo, A., Guzman, E., Hernandez, J.: Dielectric characteristics of a model transmission line in the presence of fire. IEEE Trans. Electr. Insul. 26(4), 776–782 (1991)
27. Lanoie, R., Mercure, H.: Influence of forest fires on power line insulation. In: Sixth International Symposium on High Voltage Engineering, pp. 1–4. ISH, Glasgow (1989)
28. Zohri, E., Emad H., Hamdy M. et al.: Mathematical modeling of agricultural fires beneath high voltage transmission lines. Energy 36(11), 385–396 (2011)
29. Wang, H., Zhu, J., Jiang, W., et al.: A mathematical model for estimating surface fire behavior. Fire Saf. Sci. 3(1), 33–41 (1994)
30. Zhang, X., Liu, P., Wang, X.: Research on improvement of Wang Zhengfei's forest fire spread model. J. Shandong For. Sci. Technol. 50(01), 1–6 (2020)
31. Li, C.: A Study on the Relationship between the Moisture Content of Forest Fuel and the Fire Risk Level. For. Inventory Plann. 4, 37–42 (1994)
32. Mao, X., Xu, W.: Study on calculating method of forest fire spread velocity. Meteorol. Liaoning 01, 9–13 (1991)

33. Feng, J.: Experimental study on fire spread rate characteristics of forest surface fuels in south China. Fire Sci. Technol. 41(06), 832–835 (2022)
34. Zhang, F., Xie, X.: An improved forest fire spread model and its realization. Geomatics Spat. Inf. Technol. 35(2), 50–53 (2012)
35. Zhou, Z., Ai, X., Lu, J., et al.: Real-time analysis approach and its application for transmission-line trip risk due to wildfire disaster. Proc. CSEE, 37(18), 5321–5330 (2017)
36. Zhou, Z.: Research on Risk Assessment of Power Grid Transmission-Line Trips Due to Wildfire Disasters. North China Electric Power University (2019)
37. Zhang, Z., Tian, Z., Wang, W., et al.: Expressions of the burning intensity and energy release during forest fire spread. For. Fire Prev. 3, 31–34 (2019)
38. Ning, J., Weng, Y., Di, X., et al.: Rapid determination method for swamp meadow surface fuel loads of Daxing'an Mountains. J. Northeast For. Univ. 46(05), 44–48 (2018)
39. Wu, Q., Wu, Z., Lin, S., et al.: Classification of forest fuels and prediction of fire behavior in southern Jiang xi. Chin. J. Ecol. 43(2), 314 (2024)
40. Liu, J.: Study on the characteristics of four stand types in Northern Fujian and their understory combustible matter load. For. Investig. Des. 51(05), 8–11 (2022)
41. Wu, Y.: Surface Fuel Load of Main Forest Types and its Influencing Factors in She Xian County. Anhui Agricultural University, Hefei (2022)
42. Du, J.: The Study of Algorithms for Power System Reliability Evaluation Based on Monte Carlo Simulation. Zhejiang University, Hangzhou (2015)
43. Zhao, J., Niu, H., Wang, Y.: Dynamic reconfiguration of active distribution network based on information entropy of time intervals. Power Syst. Technol. 41(2), 402–408 (2017)
44. Huang, G.: Smart Grid Dispatch Optimization for System Resilience Enhancement. Zhejiang University, Hangzhou (2018)
45. Wang, X.: Study on Spread Simukation of 4.30 Hannuohe Fire of Daxinganling Heilongjiang Province. Northeast Forestry University, Harbin (2012)
46. Zhao, N.: Resilience assessment and full-time resilience enhancement strategies for transmission system under ice disaster. Tianjin University, Tianjin (2020)

How to cite this article: Shu, S., Xiao, N., Cao, S., Xu, J., Fang, C., Xie, W.: Resilience assessment of power transmission system during wildfire disasters considering spread process. IET Gener. Transm. Distrib. 1–17 (2024). https://doi.org/10.1049/gtd2.13313